Available online at www.sciencedirect.com
ScienceDirect
Journal of the European Ceramic Society 30 (2010) 1419–1425
www.elsevier.com/locate/jeurceramsoc

The influence of the additive $BaGeO_3$ on $BaSnO_3$ ceramics

Roberto Köferstein *, Lothar Jäger, Mandy Zenkner, Thomas Müller, Stefan G. Ebbinghaus

Institut für Chemie, Anorganische Chemie, Martin-Luther-Universität Halle-Wittenberg, Kurt-Mothes Strasse 2, D-06120 Halle, Germany

Received 7 August 2009; received in revised form 16 November 2009; accepted 17 December 2009
Available online 12 January 2010

Abstract

DTA, XRD and sintering investigations of the system $BaSnO_3$–$BaGeO_3$, prepared by a mixed-oxide method, are described herein. The melting temperature of this system is about 1270 ± 5 °C. We find a partial solubility of $BaGeO_3$ into $BaSnO_3$ of the order of 6–7 mol%. Up to 50 mol% $BaGeO_3$, the calcined powders (1150 °C) as well as the once-sintered samples consist of $BaSnO_3$ and orthorhombic $BaGeO_3$ at room temperature. A gradual appearance of hexagonal $BaGeO_3$ can be observed in calcined powders and once-sintered ceramics with a $BaGeO_3$ content above 50 mol%. After sintering at ≥1200 °C for more than 1 h all ceramic bodies consist of $BaSnO_3$ and orthorhombic $BaGeO_3$. The addition of $BaGeO_3$ leads to a considerable reduction of the sintering temperature and to a strong densification. Sintering at 1180 °C for 10 h and an addition of only 1 mol% $BaGeO_3$ leads to dense ceramic bodies with cubic-like grains.

Keywords: Sintering; Perovskites; Powders-solid state reaction; Grain size; Ceramics

1. Introduction

Pure and doped barium stannate as well as its solid solutions (e.g. $BaTi_{1-x}Sn_xO_3$) have found important applications in materials science and technology due to their dielectric properties, semiconducting behaviours and high thermal stability. Because of these characteristic properties, $BaSnO_3$ based ceramics are becoming more and more important in material technology. It can be used to prepare thermally stable capacitors and to fabricate ceramic boundary layer capacitors.[1–8] Moreover, barium stannate can be also used as a functional material for semiconductor gas sensors[9–15] and photocatalytic applications.[16–18] In general, compacts on the basis of $BaSnO_3$ reveal only a moderate densification behaviour.[2,19–25] Piercy[26] obtained dense $BaSnO_3$ ceramic bodies at sintering temperatures above 1700 °C. Therefore, such ceramic bodies need high sintering temperatures or very long soaking times.[7,27] In order to produce capacitor components based on $BaSnO_3$, dense (almost pore free) material bodies are required, because pores would act as sink to the electrical charge carriers and would be the source of poor grain-to-grain connectivity and significant dielectric loss.[23,24,28–32] The addition of additives can significantly reduce the sintering temperature obtaining dense ceramic bodies due to an improvement of the densification behaviour. Wang et al.[33] used SiO_2 as a sintering aid for $BaSnO_3$ ceramics and Kumar and Choudhary[34] sintered $BaSnO_3$ at 1200 °C adding $BaSiO_3$. They found the formation of solid solutions of the type $BaSn_{1-x}Si_xO_3$ ($x = 0$–0.15). The $BaSn_{1-x}Si_xO_3$ samples show NTCR (Negative Temperature Coefficient of Resistance) behaviour and a better electrical conduction at elevated temperature than pure $BaSnO_3$ ceramic bodies. $BaGeO_3$ can be also used as a sintering aid to drastically reduce the sintering temperature to produce dense ceramic bodies as reported for $BaTiO_3$-based ceramics.[35–37] The influence and effect of the additive $BaGeO_3$ on the sintering behaviour and microstructure of $BaSnO_3$ ceramics or ceramic systems based on $BaSnO_3$ has not been investigated yet.

The aim of this work is to study the effect of $BaGeO_3$ on the sintering properties and microstructure of $BaSnO_3$ compacts. Furthermore, the formation of solid solutions and the phase evolution in the system $BaSnO_3$–$BaGeO_3$ is also investigated.

2. Experimental

2.1. Material preparation

$BaSn_{1-x}/Ge_xO_3$ powders with varying $BaGeO_3$ contents were prepared via a conventional mixed-oxide method. All

* Corresponding author. Tel.: +49 345 5525630; fax: +49 345 5527028.
E-mail address: roberto.koeferstein@chemie.uni-halle.de (R. Köferstein).

0955-2219/$ – see front matter © 2009 Elsevier Ltd. All rights reserved.
doi:10.1016/j.jeurceramsoc.2009.12.015

powders were handled in a fume hood. Equivalent amounts of $BaCO_3$ (Sabed VL 600, 99.9%, Solvay), SnO_2 (≥99.0%, Merck) and GeO_2 (99.999%, Acros Organics) were milled in a PVC container for 24 h using ZrO_2-balls and propan-2-ol (m_{powder}:m_{balls}:$m_{propan\text{-}2\text{-}ol}$ = 1:1:4). After filtering and drying the mixtures were calcined in static air (heating rate 10 K/min) for 2 h at 1150 °C.

For the shrinkage and sintering behaviour the calcined powders were milled with ZrO_2-balls and propan-2-ol in a PVC container for 2 h (m_{powder}:m_{balls} = 1:4). After filtering and drying the powders were mixed with 5 mass% of a saturated aqueous solution of polyvinyl alcohol (PVA) as a pressing aid. Then the powders were pressed to pellets with a green density of about 3.4–3.6 g/cm^3.

2.2. Analytical methods

X-ray powder diffraction (XRD) patterns were recorded by a STOE STADI MP diffractometer at 20 °C using CoKα_1 radiation. The infrared spectra were recorded on a FTIR spectrometer Mattson 5000 (Mattson Instruments Inc.) with a resolution of 2 cm^{-1} as KBr pellets. Dilatometric investigations (shrinkage) were performed in a TMA 92-16.18 unit from Setaram. Differential thermoanalytic (DTA) measurements were recorded using a Netzsch STA 449 System (heating/cooling rate 10 K/min, Pt-crucible, flowing air (20 ml/min)). Each DTA sample was measured three times to ensure reproducibility. The melting temperature was determined by the onset temperature of the DTA signal.[38]

The specific surface area was determined using nitrogen three-point BET (Nova 1000, Quantachrome Corporation). The equivalent BET particle diameter was calculated according to the equation given in Ref. 39 assuming the powder particles were spherical or cubic in shape. Scanning electron microscope images and energy dispersive X-ray analyses (EDX) were recorded with a Philips XL30 ESEM (Environmental Scanning Electron Microscope) and an attached energy dispersive X-ray spectrometer from Edax. Transmission electron microscope images were recorded with a Jeol JEM 2100F.

3. Results and discussion

3.1. Characterization of the system $BaSnO_3$–$BaGeO_3$

Mixtures of $BaCO_3$, SnO_2 and GeO_2 were heated in a Pt-crucible at 1150 °C for 2 h to obtain powders with a composition of $BaSn_{1-x}/Ge_xO_3$. Calcined powders with 1 mol% and 2 mol% $BaGeO_3$ show only reflections of the $BaSnO_3$ phase (perovskite structure) (Fig. 1). A powder with 5 mol% $BaGeO_3$ hints at very small traces of an additional orthorhombic $BaGeO_3$ phase. Up to a $BaGeO_3$ content less than 50 mol% we observe always reflections of $BaSnO_3$ and orthorhombic $BaGeO_3$. $BaGeO_3$ crystallises in two modifications. Hexagonal (α)-$BaGeO_3$ (low-temperature form) having a pseudowollastonite-type structure[40] and orthorhombic (β)-$BaGeO_3$ (high-temperature form) crystallises in a pyroxene-type structure.[41] The phase transition between these modifications appears at about 1200 °C.[42] At

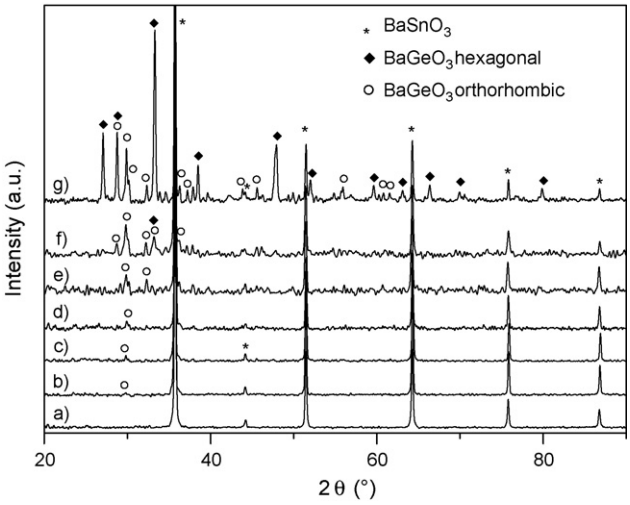

Fig. 1. XRD patterns (recorded at 20 °C) of calcined $BaSn_{1-x}/Ge_xO_3$ powders (1150 °C, 2 h) with various $BaGeO_3$ contents. (a) 1 mol%; (b) 5 mol%; (c) 10 mol%; (d) 15 mol%; (e) 30 mol%; (f) 50 mol%; (g) 80 mol%.

50 mol% $BaGeO_3$ we obtain both the orthorhombic $BaGeO_3$ phase and traces of the hexagonal one. The fraction of the hexagonal phase raises with increasing $BaGeO_3$ content. Fig. 2 shows IR spectra of calcined powders with 1 mol% and 15 mol% $BaGeO_3$, exemplarily. The peak around 1420 cm^{-1} suggests very small traces of $BaCO_3$.[43]

The above described calcined powders were the basic powders for all further investigations. After pelleting of the these powders, sintering at 1150 °C for 10 h and cooling down (10 K/min) to room temperature, ceramics with a $BaGeO_3$ content ≥50 mol% show besides the $BaSnO_3$ phase only reflections of hexagonal $BaGeO_3$ (Fig. 3). In contrast, samples with less than 50 mol% $BaGeO_3$ reveal the pattern of orthorhombic $BaGeO_3$. However, after repeated crushing and sintering at 1150 °C, the XRD patterns of these samples (<50 mol% $BaGeO_3$) reveal the formation of hexagonal $BaGeO_3$ (Fig. 3e). After sintering at 1200 °C for 10 h we observe that all ceramic samples exhibit only reflections of orthorhombic $BaGeO_3$. Up

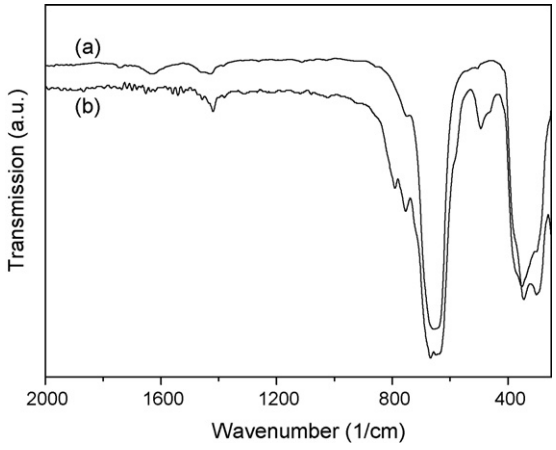

Fig. 2. IR spectra of calcined samples containing (a) 1 mol% and (b) 15 mol% $BaGeO_3$. Spectrum (a) shows a weak broad band at about 1630 cm^{-1} (δ_{OH}) due to water absorbed by the KBr powder.

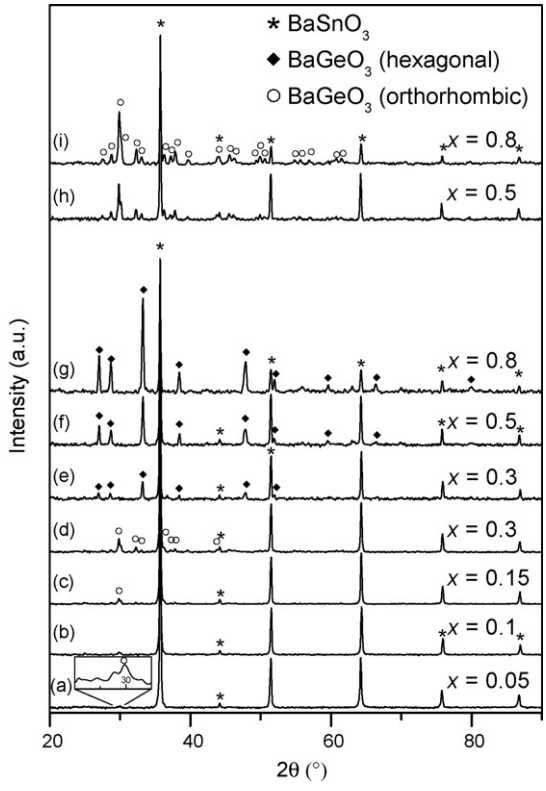

Fig. 3. XRD patterns (recorded at 20 °C) of $BaSn_{1-x}/Ge_xO_3$ ceramics after various sintering temperatures and soaking times. (a–d) 1150 °C, 10 h; (e) 1150 °C, 10 h with intermittent cooling, crushing and pelleting; (f, g) 1150 °C, 10 h; (h, i) 1200 °C, 10 h.

to 1400 °C we found as crystalline phases always both $BaSnO_3$ and $BaGeO_3$. It can be seen from Fig. 3b, that the $BaGeO_3$ phase clearly appears at samples with at least 10 mol% $BaGeO_3$ content. Sintered bodies with 5 mol% $BaGeO_3$ hint at very small traces of a $BaGeO_3$ phase. However, repeated sintering, crushing and pelleting of this sample leads to a disappearing of the $BaGeO_3$ reflections and thus to a complete formation of a solid solution between the non-isotypic compounds $BaSnO_3$ and $BaGeO_3$.

For the following DTA and EDX measurements the calcined samples were pressed to pellets, sintered several times with intermittent cooling, crushing and re-pelleting. EDX measurements of several grains in various ceramic bodies suggest a solid solubility of $BaGeO_3$ into the $BaSnO_3$ structure of about 6–7 mol%, which confirm the above XRD results. Because of the limited solid solubility, we describe the system $BaSnO_3$–$BaGeO_3$ by the formula $BaSn_{1-x}/Ge_xO_3$.

DTA investigations of pure $BaGeO_3$ indicated a melting point of 1290 ± 5 °C (Fig. 4) and a hexagonal ⇆ orthorhombic phase transition temperature of 1190 ± 5 °C (not shown in Fig. 4) in good agreement with earlier data.[42,44] $BaSnO_3$ has a very high melting point, which could not be determined by us. However, Wagner and Binder[45] reported a melting temperature of 2057 °C. DTA measurements of $BaSn_{1-x}/Ge_xO_3$ samples with various $BaGeO_3$ contents ($x \geq 0.1$) reveal a melting temperature at about 1270 ± 5 °C (Fig. 4). Samples with a $BaGeO_3$ concentration below 10 mol% do not show any melting peak.

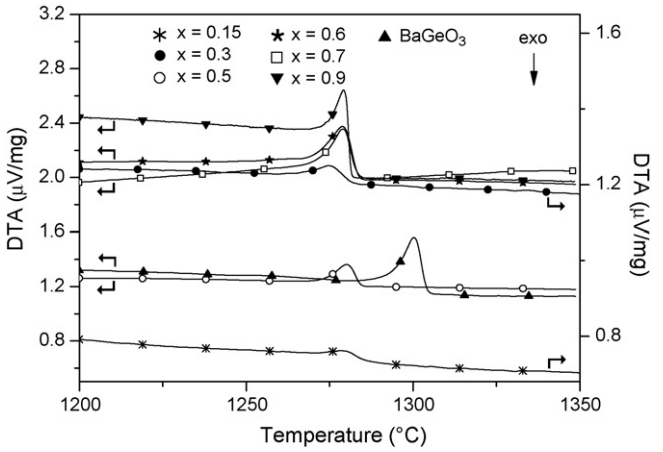

Fig. 4. DTA traces (melting point) of $BaGeO_3$ and various $BaSn_{1-x}/Ge_xO_3$ ($x \geq 0.15$) samples.

3.2. Shrinkage and sintering behaviour

Four different preceramic powders were used for these investigations. Powders with $BaGeO_3$ contents of 1 mol% (**1**), 2 mol% (**2**), 5 mol% (**5**) and 15 mol% (**15**) were obtained after calcination at 1150 °C for 2 h (heating rate 10 K/min), as described above. The specific surface areas and the equivalent BET particle diameters of these powders are given in Table 1. It can be seen that an increasing $BaGeO_3$ content causes a decreasing specific surface area and thus a raising BET particle diameter, which can be considered as an average size of the primary particles.[46] Fig. 5 shows the cubic- and cuboid-like morphology of powder **1**. The particles of this powder are strong agglomerated (Fig. 5b). The theoretical bulk densities of the resulting ceramic bodies were calculated as 7.22 g/cm^3 (**1**), 7.19 g/cm^3 (**2**), 7.12 g/cm^3 (**5**) and 6.85 g/cm^3 (**15**).[47]

The shrinkage behaviour of green bodies of **1**, **5** and **15** are depicted in Fig. 6. Sample **1** slowly starts to shrink at about 1050 °C and the maximum shrinkage rate is observed at 1295 °C (−2.3%/min). Further addition of $BaGeO_3$ leads to a shift of the maximum shrinkage rate to 1265 °C (−1.8%/min) (**5**). The maximum shrinkage rate in sample **15** is characterized by a sharp asymmetric peak. The peak at 1280 °C exhibits an approximately two times higher shrinkage rate (−3.8%/min) and is assigned to the formation of a liquid phase. In samples with a $BaGeO_3$ content >15 mol% we observe the appearance of two separate peaks; a first peak in the range 1200–1215 °C and a second one at about 1280 °C. The shrinkage of sample **5** slowly starts at 950 °C, however a significant shrinkage occurs above

Table 1
Properties of $BaSn_{1-x}/Ge_xO_3$ powders calcined at 1150 °C for 2 h.

Powder	$BaGeO_3$ content (mol%)	BET specific surface area (m^2/g)	Average particle diameter[a] (nm)
1	1	3.9	213
2	2	2.7	309
5	5	2.4	351
15	15	1.5	581

[a] Calculated from the specific surface area.[39]

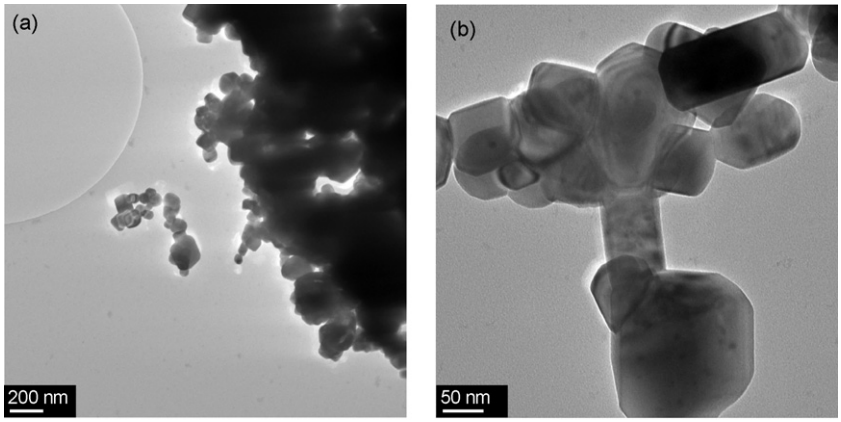

Fig. 5. TEM images of powder **1**.

1060 °C, whereas the sample containing 15 mol% $BaGeO_3$ (**15**) starts to shrink not until about 1040 °C. Compared to pure $BaSnO_3$ samples[19] the addition of $BaGeO_3$ causes considerably higher shrinkage rates and thus stronger shrinkage at lower temperatures.

Fig. 7 shows the final bulk densities of $BaSn_{1-x}/Ge_xO_3$ ($x = 0.01$ (**1**); 0.02 (**2**); 0.05 (**5**); 0.15 (**15**)) ceramics after isothermal sintering between 1150 °C and 1400 °C for 1 h and 10 h, respectively. Up to 1200 °C and a soaking time of 1 h ceramic bodies with a relative density of 76–87% can be obtained. Dense ceramic bodies (relative density ≥90%) can be obtained at temperatures above 1200 °C. As seen in Fig. 7, after sintering of 1 h ceramics of **1**, **2** and **5** achieve at 1230 °C relative densities of 92% (6.62 g/cm^3), 91% (6.53 g/cm^3) and 93% (6.65 g/cm^3), respectively. Sample **15** requires a sintering temperature of 1250 °C to form dense ceramic bodies. Higher sintering temperatures lead only to a marginal increase in density. A prolonged soaking time of 10 h results in a slight reduction of the required sintering temperature for dense ceramic bodies. After 10 h and a temperature of 1180 °C we obtain ceramics with densities of 6.52 g/cm^3 (90%, **1**), 6.52 g/cm^3 (91%, **2**), 6.44 g/cm^3 (90%, **5**) and 5.58 g/cm^3 (81%, **15**). Above 1150 °C the final relative densities of ceramics **1**, **2** and **5** differ only slightly from each other, whereas ceramic bodies of **15** exhibit lower relative densities. The general decrease in absolute densities of $BaSn_{1-x}/Ge_xO_3$ ceramics with increasing $BaGeO_3$ content is

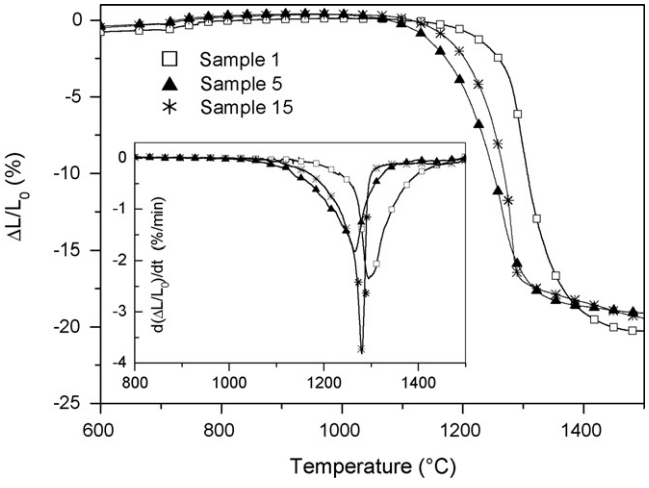

Fig. 6. Shrinkage behaviour (non-isothermal, heating rate 10 K/min) of green bodies of **1**, **5** and **15**. The inset shows the relative shrinkage rate ($d(\Delta L/L_0)/dt$) of these bodies.

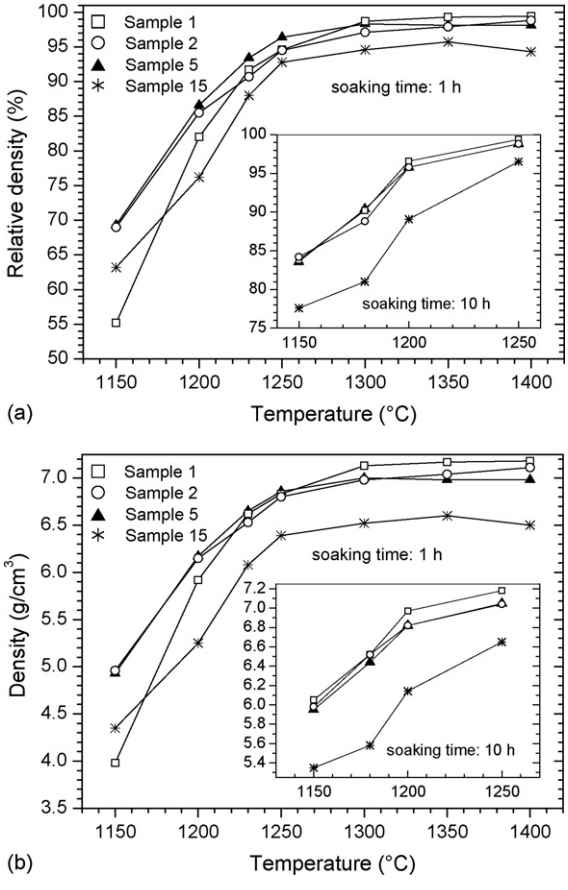

Fig. 7. Final densities of $BaSn_{1-x}/Ge_xO_3$ ceramic bodies of **1** ($x = 0.01$), **2** ($x = 0.02$), **5** ($x = 0.05$) and **15** ($x = 0.15$) after an isothermal sintering process at various temperatures at the indicated soaking times in a muffle furnace (heating/cooling rate: 10 K/min). (a) Relative densities vs. sintering temperature and (b) absolute densities vs. sintering temperature. The relative densities are related to the theoretical density of 7.22 g/cm^3 (**1**), 7.19 g/cm^3 (**2**), 7.12 g/cm^3 (**5**) and 6.85 g/cm^3 (**15**).

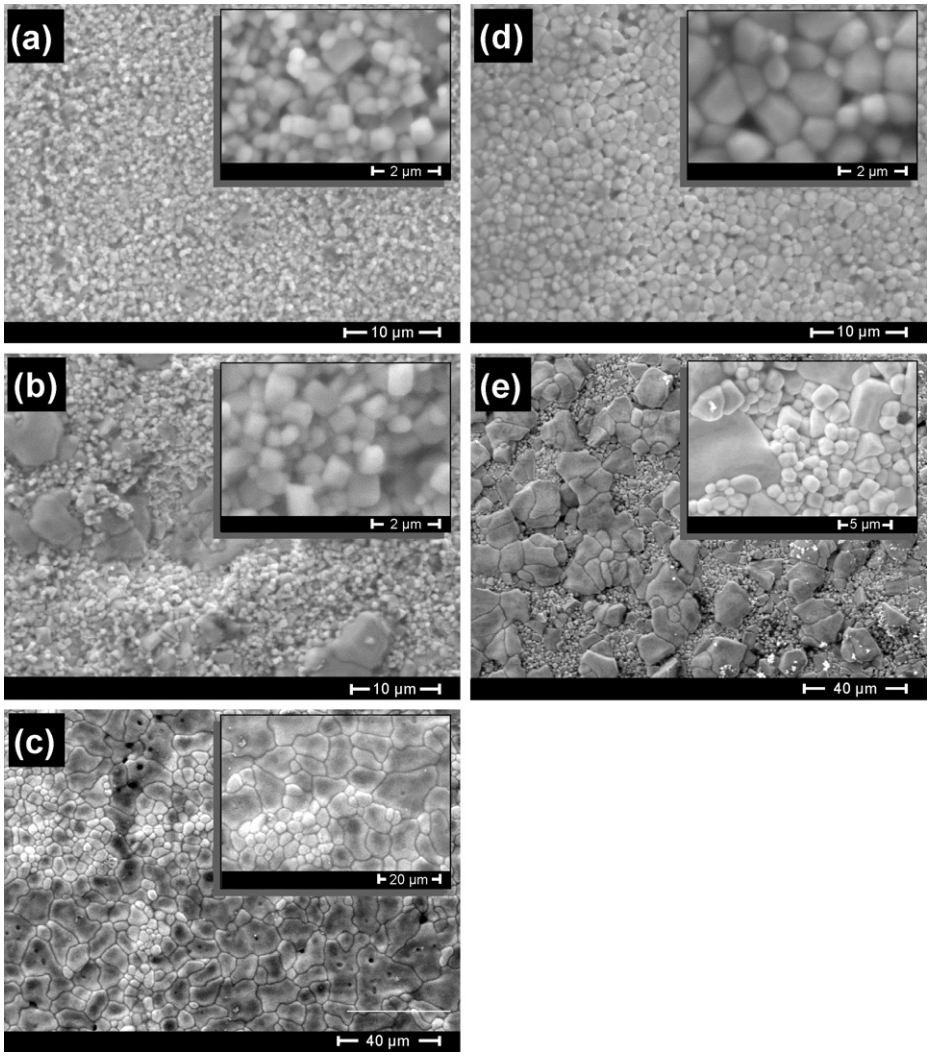

Fig. 8. SEM micrographs of the surfaces of ceramic bodies of **1** after various sintering temperatures and soaking times. (a) 1230 °C, 1 h; (b) 1300 °C, 1 h; (c) 1400 °C, 1 h; (d) 1180 °C, 10 h; (e) 1250 °C, 10 h.

also due to the reduction of the maximum achievable density by adding $BaGeO_3$ (see above).

As seen in Fig. 3c ceramic bodies of **15** consist of orthorhombic $BaGeO_3$ besides $BaSnO_3$ as the main crystalline phase.

From the outlined results it can be concluded that an amount of 1 mol% $BaGeO_3$ is sufficient to obtain dense $BaSn_{1-x}/Ge_xO_3$ ceramic bodies at low sintering temperatures.

The micrographs of ceramics of **1** are shown in Fig. 8. Sintering at 1230 °C for 1 h of **1** results in ceramic bodies with cubic-like grains of about 0.3–1.3 μm (∅ = 0.7 μm[48]), whereas ceramic bodies of **15** (not shown in Fig. 8) reveal grain sizes between 0.5 μm and 1.8 μm. A sintering temperature of 1300 °C for 1 h (Fig. 8b) reveal in both samples a bimodal or heterogeneous grain size distribution with grain sizes of about 0.5–1 μm/2.5–7 μm (**1**) and 0.7–6 μm (**15**). Sintering at 1400 °C (Fig. 8c) leads also to a bimodal microstructure with irregular grains between 2.5 μm and 26 μm (**1**). An increasing soaking time to 10 h at 1180 °C causes for ceramics of **1** a homogeneous microstructure with grains between 0.4 μm and 2 μm (∅ = 1.6 μm) (Fig. 8d) and in sample **15** we find grains in the range 0.8–2.8 μm. Sintering at 1250 °C for 10 h (Fig. 8e) leads in both samples (**1**, **15**) to a bi-modal grain growth with grain fractions of 0.8–2 μm and 5–20 μm (**1**) or to a heterogeneous microstructure with grains between 1 μm and 15 μm (**15**). The smaller grain fractions mainly consist of cubic-like grains, whereas the larger grains have a more irregular shape as seen from the inset in Fig. 8e.

The isothermal sintering clearly shows, that dense ceramic bodies can be obtained at sintering temperatures below the formation of the liquid phase (<1270 °C). This indicated that the formation of a liquid phase is not essential for densification of the investigated ceramic bodies. Therefore, the additive $BaGeO_3$ does not affect primarily as a liquid phase former, but it improves the sintering behaviour by sliding processes (viscous flow). Fig. 9 exemplarily shows the result of isothermal dilatometric investigations of compacts of **2** and **15**. By means of the general shrinkage Eq. (1),[49] a logarithmic representation of $\Delta L/L_0$ vs. time (t) allows to determine the dominant shrinkage

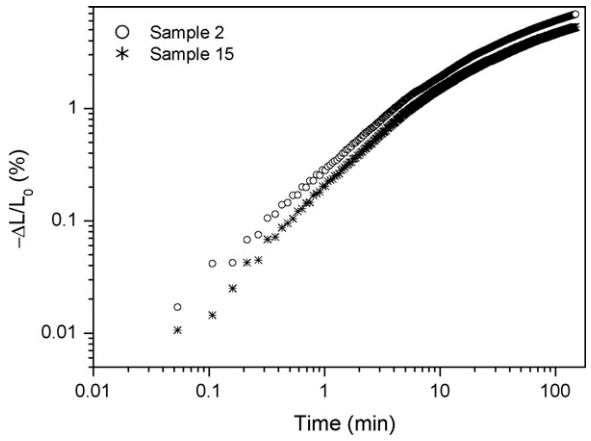

Fig. 9. Isothermal dilatometric investigations demonstrated at 1150 °C for green bodies of **2** and **15**. The figure shows a double logarithmic plot of $\Delta L/L_0$ vs. time (t) of the isothermal segments (the initial values were set to zero).

mechanisms:

$$\left(\frac{\Delta L}{L_0}\right)^{m/2} = -\frac{H}{2^m R^n} t \quad (1)$$

Here, $\Delta L/L_0$ is the relative shrinkage, H is a function containing material parameters, R is the radius of the particles, t is the time, n and m are numerical exponents depending on the shrinkage mechanism.

The isothermal part clearly shows that the isothermal shrinkage process is divided into two sections representing two different shrinkage mechanisms.[35,50] The first segment of the isothermal curves has a slope according to a shrinkage exponent of about $m = 2$ indicating viscous flow as the major shrinkage mechanism. The second segment ($m = 4$–6) suggests grain boundary diffusion and volume diffusion from the grain boundaries as the dominant shrinkage process. It can be seen that the beginning of the shrinkage process is dominated by sliding processes (viscous flow). Such processes are caused by defect-rich and amorphous (glass-like) contact boundaries.[51–53] The sliding processes of whole grains are supported by $BaGeO_3$ and result in a reducing sintering temperature. A similar improved densification behaviour during solid-state sintering by addition of germanium- and silicon-based additives is also observed in $BaTiO_3$ ceramics.[35,50]

4. Conclusion

The system $BaSnO_3$–$BaGeO_3$ ($BaSn_{1-x}/Ge_xO_3$, $x \geq 0.1$) reveals a melting temperature of about 1270 ± 5 °C. XRD investigations and EDX measurements of single grains of various ceramic bodies suggest a solubility of $BaGeO_3$ in $BaSnO_3$ of the order of 6–7 mol%. $BaSn_{1-x}/Ge_xO_3$ samples ($x \geq 0.1$) heated up to 1400 °C show reflections of both a $BaSnO_3$ phase and a $BaGeO_3$ one, whereas samples with $x < 0.1$ reveal only reflections of the $BaSnO_3$ phase.

$BaGeO_3$ can be used as a sintering additive for $BaSnO_3$ ceramics to reduce the sintering temperature. The ceramic bodies were prepared from mixed-oxide powders (calcined at 1150 °C, 2 h). The sintering behaviour was studied on samples containing 1–15 mol% $BaGeO_3$. An addition of 1 mol% $BaGeO_3$ is sufficient to obtain dense ceramic bodies (relative density ≥90%) after a conventional solid state sintering process of 1 h at 1230 °C, or 10 h at 1180 °C. Raising sintering temperatures or an increased $BaGeO_3$ content promote the formation of an heterogeneous or bimodal grain size distribution in the ceramic bodies.

Acknowledgements

The authors would like to thank Mr. F. Syrowatka for EDX measurements. We are also grateful to Dr. Garcia (University of Augsburg) for making TEM images. Financial support by the Federal State Saxony-Anhalt (Cluster of Excellence "Nanostructured Materials") is gratefully acknowledged.

References

1. Vivekanandan R, Kutty TRN. Grain boundary layer ceramic capacitors based on donor-doped $Ba(Ti_{1-x}Sn_x)O_3$. *Mater Sci Eng B* 1990;**6**(4):221–31.
2. Singh P, Brandenburg BJ, Sebastian CP, Singh P, Singh S, Kumar D, et al. Electronic structure, electrical and dielectric properties of $BaSnO_3$ below 300 K. *Jpn J Appl Phys* 2008;**47**:3540–5.
3. Movchikova A, Malyshkina O, Suchaneck G, Gerlach G, Steinhausen R, Langhammer HT, et al. Study of the pyroelectric behavior of $BaTi_{1-x}Sn_xO_3$ piezo-ceramics. *J Electroceram* 2008;**20**:43–6.
4. Wang T, Chen XM, Zheng XH. Dielectric characteristics and tunability of barium stannate titanate ceramics. *J Electroceram* 2003;**11**:173–8.
5. Kumar A, Singh BP, Choudhary RNP, Thakur AK. Ferroelectric phase transition in Te-modified $BaSnO_3$. *Mater Lett* 2005;**59**:1880–8.
6. Prokopalo OI. Conductivity and anomalous polarization in ceramicferroelectrics with perovskite structure. *Ferroelectrics* 1976;**14**:683–5.
7. Singh P, Kumar D, Parkash O. Dielectric behavior of the system $BaSn_{1-x}Nb_xO_3$ ($x \leq 0.10$). *J Appl Phys* 2005;**97**. p. 074103.
8. Brauer H. Korngrenzensperrschichten in $BaTiO_3$ Keramik mit hoher effektiver Dielektrizitätskonstante. *Z Angew Phys* 1970;**29**:282–7.
9. Ostrick B, Fleischer M, Lampe U, Meixner H. Preparation of stoichiometric barium stannate thin films: hall measurements and gas sensitivities. *Sens Actuators B* 1997;**44**:601–6.
10. Tao S, Gao F, Liu X, Sørensen OT. Ethanol-sensing characteristics of barium stannate prepared by chemical precipitation. *Sens Actuators B* 2000;**71**:223–7.
11. Hodjati S, Vaezzadeh K, Petit C, Pitchon V, Kiennemann A. NO*x* sorption–desorption study: application to diesel and lean-burn exhaust gas (selective NO*x* recirculation technique). *Catal Today* 2000;**59**:323–34.
12. McGeehin P, Williams D.E. Sensing gaseous substances. *Int. Appl.*, Patent No. WO 9308467 A1 19930429; 1993.
13. Gopal Reddy V, Manorama SV, Rao VJ. Preparation and characterization of barium stannate: application as a liquefied petroleum gas sensor. *J Mater Sci: Mater Electron* 2001;**12**:137–42.
14. Upadhyay S, Kavitha P. Lanthanum doped barium stannate for humidity sensor. *Mater Lett* 2007;**61**:1912–5.
15. Cerda J, Arbiol J, Dezanneau G, Diaz R, Morante JR. Perovskite-type $BaSnO_3$ powders for high temperature gas sensor applications. *Sens Actuators B* 2002;**84**:21–5.
16. Borse PH, Joshi UA, Ji SM, Jang JS, Lee JS, Jeong ED, et al. Band gap tuning of lead-substituted $BaSnO_3$ for visible light photocatalysis. *Appl Phys Lett* 2007;**90**. p. 034103-1.
17. Yuan Y, Lv J, Jiang X, Li Z, Yu T, Zou Z, et al. Large impact of strontium substitution on photocatalytic water splitting activity of $BaSnO_3$. *Appl Phys Lett* 2007;**91**. p. 094107-1.
18. Zhang Y, Zhang H, Wang Y, Zhang WF. Efficient visible spectrum sensitization of $BaSnO_3$ nanoparticles with N719. *J Phys Chem C* 2008;**112**:8553–7.

19. Köferstein R, Jäger L, Zenkner M, Ebbinghaus SG. Nano-sized $BaSnO_3$ powder via a precursor route. Comparative study of sintering behaviour and mechanism of fine and coarse-grained powders. *J Eur Ceram Soc* 2009;**29**:2317–24.
20. Singh P, Kumar D, Parkash O. DC conduction behaviour of niobium doped barium stannate. *J Mater Sci: Mater Electron* 2005;**16**:145–8.
21. Upadhyay S, Parkash O, Kumar D. Dielectric relaxion and conduction in the system $Ba_{1-x}La_xSn_{1-x}Cr_xO_3$. *J Mater Sci: Mater Electron* 2001;**12**:165–72.
22. Wie X, Yao X. Preparation, structure and dielectric property of barium stannate titanate ceramics. *Mater Sci Eng B* 2007;**137**:184–8.
23. Cernea M, Manea A, Piazza D, Galassi C, Vasile E. $Ba(Ti_{1-x}Sn_x)O_3$ ($x=0.13$) dielectric ceramics prepared by coprecipitation. *J Am Ceram Soc* 2007;**90**:1728–32.
24. Azad A-M, Hon NC. Characterization of $BaSnO_3$-based ceramics. Part 1. Synthesis, processing and microstructural development. *J Alloys Comp* 1998;**270**:95–106.
25. Tien L-C, Chou C-C, Tsai D-S. Microstructure of $Ba(Mg1/3Ta2/3)O_3$–$BaSnO_3$ microwave dielectrics. *Ceram Int* 2000;**26**:57–62.
26. Piercy B. Dielectric properties of some polycrystalline stannates and cerates. *Trans Faraday Soc* 1959;**55**:39–51.
27. Cava J, Gammel P, Batlogg B, Krajewski JJ, Peck Jr WF, Rupp Jr WL, et al. Nonsuperconducting $BaSn_{1-x}Sb_xO_3$: the 5s-orbital analogue of $BaPb_{1-x}Bi_xO_3$. *Phys Rev B* 1990;**42**:4815–8.
28. Rice RW. *Porosity of ceramics*. New York: Marcel Dekker; 1998. p. 325 et seqq.
29. Marković S, Mitrić M, Cvjetićanin N, Uskoković D. Structural and dielectric properties of $BaTi_{1-x}Sn_xO_3$ ceramics. *Mater Sci Forum* 2006;**518**:241–6.
30. Singh P, Parkash O, Kumar D. Electrical conduction behaviour of perovskite oxide system $BaSn_{1-x}Nb_xO_3$. *Solid State Ionics* 2005;**176**:2167–70.
31. He Z, Ma J, Zhang R. Investigation on the microstructure and ferroelectric properties of porous PZT ceramics. *Ceram Int* 2004;**30**:1353–6.
32. Iddles DM, Bell AJ, Moulson AJ. Relationships between dopants, microstructure and the microwave dielectric properties of ZrO_2–TiO_2–SnO_2 ceramics. *J Mater Sci* 1992;**27**:6303–10.
33. Wang Z, Zhou F, Chen Z. Preparation and electric properties of $BaSnO_3$ ceramics. *Dianzi Yuanjian Yu Cailiao* 2006;**25**:58–60.
34. Kumar A, Choudhary RNP. Characterization of electrical behaviour of Si modified $BaSnO_3$ electroceramics using impedance analysis. *J Mater Sci* 2007;**42**:2476–85.
35. Köferstein R, Jäger L, Zenkner M, Müller T, Abicht H-P. Shrinkage mechanism and phase evolution of fine-grain $BaTiO_3$ powder compacts containing 10 mol% $BaGeO_3$ prepared via a precursor route. *Mater Chem Phys* 2008;**112**:531–5.
36. Zenkner M, Jäger L, Köferstein R, Abicht H-P. Synthesis and characterization of nanoscaled $Ba(Ti_{1-x-y}Sn_xGe_y)O_3$ powders and corresponding ceramics. *Solid State Sci* 2008;**10**:1556–62.
37. Köferstein R, Jäger L, Zenkner M, Abicht H-P. Preparation and sintering behaviour of a fine grain $BaTiO_3$ powder containing 10 mol% $BaGeO_3$. *J Mater Sci* 2008;**43**:832–8.
38. Cammenga HK, Epple M. Grundlagen der Thermischen Analysetechniken und ihre Anwendungen in der präparativen Chemie. *Angew Chem* 1995;**107**:1284–301.
39. Allred VD, Buxton SR, McBride JP. Characteristic properties of thorium oxide particles. *J Phys Chem* 1957;**61**:117–20.
40. Liebau F. Zur Kristallchemie der Silikate, Germanate. Fluoberyllate des Formeltyps ABX_3. *Neues Jahrb Miner* 1960;**94**:1209–22.
41. Hilmar W. Die Struktur der Hochtemperaturform des Bariumgermanates $BaGeO_3$ (h). *Acta Crystallogr* 1962;**15**:1101–5.
42. Guha JP, Kolar D, Porenta A. Polymorphic modifications of barium metagermanate. *J Therm Anal* 1976;**9**:37–41.
43. Nakamoto K. *Infrared and Raman spectra of inorganic and coordination compounds*. USA: John Wiley & Sons; 1979. p. 129.
44. Guha JP, Kolar D. Phase equilibria in the system $BaTiO_3$–$BaGeO_3$. *J Mater Sci* 1972;**7**:1192–6.
45. Wagner G, Binder H. Untersuchung der binären Systeme BaO–SnO_2 and BaO–PbO_2. I. Phasenanalysen. *Z Allg Anorg Chem* 1958;**297**:328–46.
46. Buscaglia MT, Bassoli M, Buscaglia V, Alessio R. Solid-State synthesis of ultrafine $BaTiO_3$ powders from nanocrystalline $BaCO_3$ and TiO_2. *J Am Ceram Soc* 2005;**88**(9):2374–9.
47. Marks GW, Monson LA. Effect of certain group IV oxides on dielectric constant and dissipation factor of barium titanate. *Ind Eng Chem* 1955;**47**(8):1611–20.
48. Wurst JC, Nelson JA. Lineal intercept technique for measuring grain size in two-phase polycrystalline ceramics. *J Am Ceram Soc* 1972;**55**:109.
49. Rahaman MN. *Ceramic proceeding and sintering*. New York: Marcel Dekker; 1995. p. 398 et seqq.
50. Völtzke D, Abicht H-P. The influence of different additives and the mode of their addition on the sintering behaviour and the properties of semiconducting barium titanate ceramics. *Solid State Sci* 2000;**2**:149–59.
51. Geguzin YaE, Klinchuk YuI. Mechanism and kinetics of the initial stage of the solid-phase sintering of pressed parts from crystal-body powders activity during sintering. *Poroshkovaya Metallurgiya* 1976;**7**:17–25.
52. Schatt W. Vorgänge beim Festphasensintern und ihre Verallgemeinerungsfähigkeit. *Z Metallkde* 1989;**80**(11):809–16.
53. Schatt W. Study of sintering processes by positron annihilation. *Solid State Phenom* 1992;**25–26**:23–8.